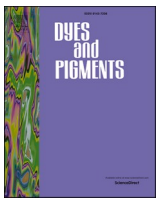
Dyes and Pigments 239 (2025) 112786



Contents lists available at ScienceDirect

Dyes and Pigments

journal homepage: www.elsevier.com/locate/dyepig



A biodegradable and biocompatibile polymer-shell to develop a H_2S sensing device

Alessio Trerotola [a], Paola Rizzo [a,*], Angela Erbaggio [a], Viktoriia Vykhovanets [a], Alessandro Landi [a], Marina Lamberti [a], Carmine di Fiore [b], Claudio Pellecchia [a], Maria Strianese [a,**]

[a] Dipartimento di Chimica e Biologia "Adolfo Zambelli"and INSTM Research Unit, Università degli Studi di Salerno, Via Giovanni Paolo II, 132, 84084, Fisciano, SA, Italy
[b] M. A. Plastic Engineering Srl, Via Cattaneo, 33, Gallarate, Va, Italy

A B S T R A C T

In this contribution we report a new family of fluorescent complexes suitable as H_2S sensors: their structural common unit is the pyridine group within the Zn-chelating ligands. Structures containing pyridines with other π-conjugated motifs represent easily accessible fluorescent materials with excellent optical properties. The successful adsorption of the developed sensors in a biocompatible and biodegradable polymer, such as Poly(butylene succinate) (PBS), provides proof-of-principle for the application of the new materials in the field of H_2S (bio) sensing and more in general of the optical sensing.

1. Introduction

H_2S plays key roles in a variety of physiological and pathophysiological conditions within the human body [1–3] and, as a consequence of the multiplicity of environments in which this molecule is found and of the multifaceted roles it covers, the interest in probes capable of detecting and eventually quantifying its amount increased a lot in the last decades [4–7]. In particular fluorescence-based approaches have witnessed an upsurge of interest [8–11].

Fluorescence is by far a dominant analytical approach, largely used in the field of environmental contaminants detection, in the discovery of new drugs, in advancing the study of biology, pathology, and medicine. Luminescent probes with high sensitivity and selectivity find application in automated detection and implementation of sensors [12]. Examples of compounds with interesting photophysical properties are coumarin derivatives [13,14], diketopyrrolopyrroles [15], Nile red-type dyes [16], BODIPYs [17,18], 1,8-naphthalimides [19,20], benzothiadiazoles [21,22], polycyclic aromatic hydrocarbons [23], styrenes [24,25], and triarylamines [26–32] but often the complexities of their synthesis and modification of their structures can inhibit their applications. Therefore, it remains a challenging task to identify new organic fluorescent materials possessing distinctive structural features which can be easily prepared [33].

Linking pyridines with other π-conjugated motifs can provide a simple and efficient means for preparing highly fluorescent organic frameworks [33] which can eventually act as metal-chelating ligands. Drawing upon these considerations, a few years ago, we reported a family of imidazo-pyridine-zinc complexes which efficiently function as fluorescent sensors for H_2S and provided evidence of their potential to visualize exogenous H_2S in biological environments [34].

Considering that salen-zinc complexes have been widely used as fluorescent sensors for different applications [35–38] and that in the course of our studies, we targeted them as probes for HS^- detection by harnessing a 'coordinative-based approach' both *in vitro* and *in vivo* [39–44], our idea for the present work, was to introduce the pyridine fragment into a 'salen-like' ligand structure (with the pyridine exerting different roles within the ligand framework) and assess the potential of the resulting zinc complexes as fluorescent H_2S sensors.

Indeed with a coordinative-based approach one may, in principle, be able to remove H_2S from the metal center of the sensor and ensure a reversible H_2S binding process. This would be advantageous for practical sensing applications, allowing reusability of the sensing device.

Fig. 1 displays the family of complexes under investigation in the current contribution.

Furthermore since we recently reported the successful sorption of fluorescent salen complexes in NC sulfonated PPO films and the ability of the related films to function as resistant and reusable solid-state devices for HS^- detection [12], we thought of applying a similar approach

* Corresponding author.
** Corresponding author.
E-mail addresses: prizzo@unisa.it (P. Rizzo), mstriane@unisa.it (M. Strianese).

https://doi.org/10.1016/j.dyepig.2025.112786
Received 14 February 2025; Received in revised form 25 March 2025; Accepted 25 March 2025
Available online 26 March 2025
0143-7208/© 2025 The Authors. Published by Elsevier Ltd. This is an open access article under the CC BY license (http://creativecommons.org/licenses/by/4.0/).

in this work but using biocompatible and biodegradable polymer films based on [Poly(butylene succinate)] PBS for the immobilization of the sensing complex.

PBS is a semi-crystalline polyester, soft and flexible with melting temperature around 110 to 115 °C and with a good thermal resistance and heat deflection temperature (HDT) of more than 90 °C. It is recognized as one of the most adaptable within compostable polymers due to the good compromise between mechanical strength, ductility, toughness and impact resistance [45–47]. PBS as well as PBS-based copolymers are widely studied and proposed for applications in different fields, such as for example in the packaging field, for the production of films for food and cosmetic packaging; in agriculture, for the manufacture of mulching films, in tissue engineering, with the polymers in the form of films as well as scaffolds, or as microspheres for realizing drug delivery systems [48,49].

Recently, PBS-based memory devices have been investigated: a switching memory was implemented on a biodegradable Ecoflex elastomeric substrate using poly(fluorene)/poly(butylene succinate) (PFN/PBS) blend films with a high potential in green electronics [50].

Herein we propose the fabrication and optimization of a flexible sensor based on polybutylene succinate (PBS) as a H_2S sensing device, the material stands out for being low-cost, flexible, biocompatible, biodegradable and easily recyclable after use. In addition, the present sensor exploits a coordinative-based approach in combination with an-easy-to-set-up and commercially available polymer, both advantageous features for practical sensing applications.

2. Results and discussion

Complexes **1**–**4** were synthesized by literature procedures [39,42,43,51,52] and characterized by high-resolution MALDI Fourier transform ion cyclotron resonance mass spectrometry (Figs. S1–S6 in the SI) and ^{1}H NMR spectroscopy (Figs. S7–S10 in the SI). MALDI and NMR experiments provide evidence that all the complexes under investigation exhibit the expected structures with complexes **1** and **2** forming mainly the dimeric species (Figs. S1–S4). The scarce solubility of complex **1** in most NMR solvents (which causes the low resolution of the ^{1}H NMR spectrum, see Fig. S7) could be likely due to its tendency to persist in the dimeric form. Complexes **3** and **4** share the same starting ligand: while for complex **3** the ligand acts as a planar tetradentate chelating ligand coordinating the zinc center through the imine and the pyridine nitrogen atoms, in complex **4**, one bis-deprotonated ligand coordinates to two different zinc metal centers, as already reported in the literature [51].

First, to assess the reactivity of the synthesized complexes with HS^-, we investigated the reactions *via* ^{1}H NMR spectroscopy. For complexes **1**–**3** the analysis of the proton spectra reveals the formation of the HS-binding adducts: both for complex **1** and for complex **3** the appearance of the characteristic high field-shifted signals of the Zn-SH protons [53,54] plus the shift of the proton resonances of the ligand moieties occur (figs S11 and fig S13). However, a close inspection of the spectrum of complex **1** (Fig. S11) in the presence of HS^-, suggests that the formation of different species, together with the HS^- binding adduct, occurs, as evidenced by the appearance of diverse signals around 10 ppm which are likely ascribable to imine protons of different species. In addition, for complex **3** (Figs. S13 and S25) the integral of the Zn-HS signal suggests the substitution of both the chlorines. In the case of complex **2** the high field resonance of the Zn-SH proton is missing (Fig. S12) but this finding is not new and was already observed for spectra of HS^- binding adducts of complexes with OH groups on the ligand structure [34]: an exchange between the SH groups with the OH, mediated by the trace amounts of water in deuterated DMSO, occurs. As for complex **4** de-metalation of the complex occurs (e.g. the ^{1}H NMR spectrum of complex **4** upon treatment with HS^- closely resembles that of the free ligand, Fig. S14).

In the case of complexes **1** and **2** MALDI spectra of the complexes after the treatment with HS^- (Figs. S15 and S16) corroborate the results drawn by NMR: the peaks at 512.041 and at 444.001 *m/z* units are consistent with the mononuclear [complex **1**/HS]$^-$ and [complex **2**/HS]$^-$ species. Differently for complex **3**, despite several tentatives, we could not acquire the MALDI spectrum of the HS^- binding adduct.

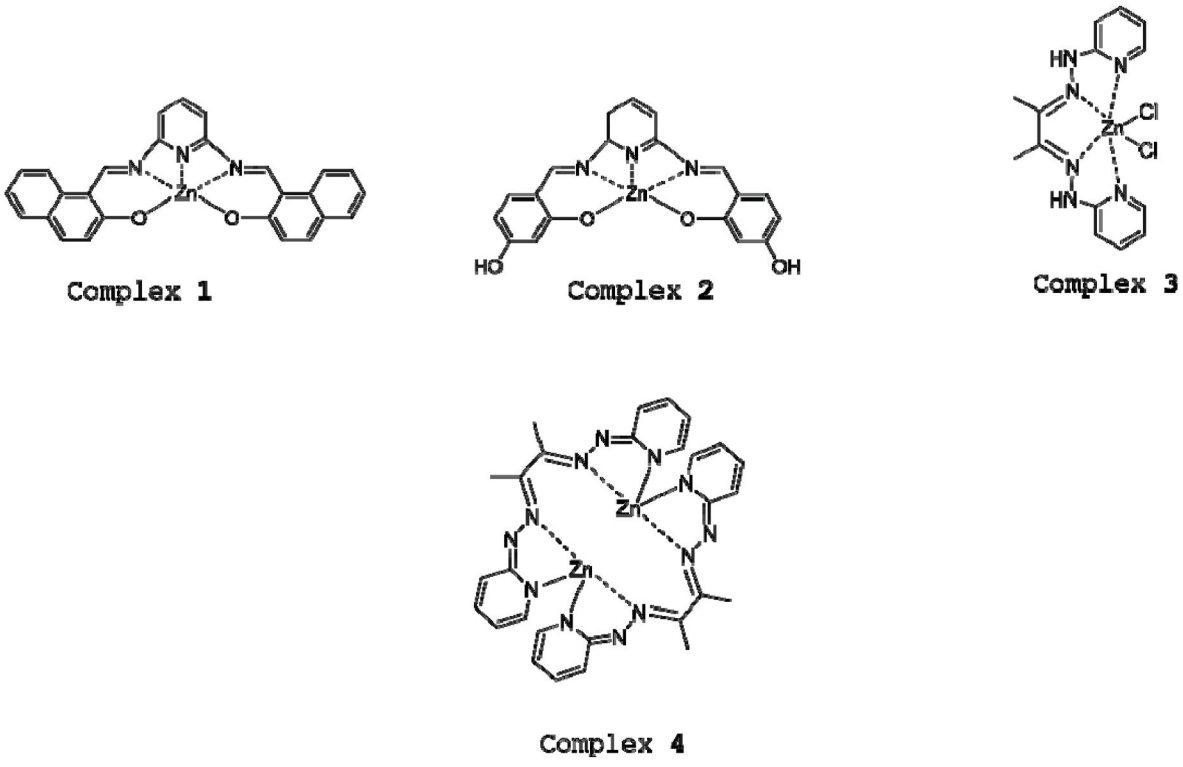


Fig. 1. Chemical structures of complexes **1**–**4** studied in this work.

To further investigate reactivity of complexes **1**–**4** with HS^- we monitored the reactions via Uv–vis and fluorescence spectroscopies. Fig. 2 displays the optical absorption spectra of complexes **1**–**4** before and after interaction with HS^-. All the complexes exhibit ligand-centered (LC) transition bands which experience visible changes upon reaction with HS^-, suggesting the formation of new species.

As already observed *via* NMR spectroscopy (Fig. S14), only in the case of complex **4** the presence of HS^- results into the leaching of the organic ligand (see Fig. S17).

Next, we studied the fluorescence responses of the complexes to HS^-: Fig. 3 displays the results.

Upon addition of HS^- an enhancement of the fluorescence intensity was observed for complex **1** whereas both complex **2** and complex **3** experience a fluorescence-turn-off. Complex **4** was found not fluorescent in the experimental conditions tested.

Thus, for the next set of experiments, we focused on complex **1** (which turns its fluorescence in the presence of the target analyte: turn-on sensors are inherently more sensitive than turn-off ones and more effective for practical measurements).

To assess whether the fluorescence response of complex **1** depends on the HS^- concentration we monitored the change of the initial fluorescence intensity after the addition of increasing concentrations of NaSH. The response of the fluorescence switchings for a series of subsequent measurements with increased concentrations of NaSH, increases accordingly (see Fig. S18 in the SI).

To obtain an indication on the selectivity of complex **1** for HS^- recognition, its fluorescence intensity in the presence of biologically relevant and potentially competing thiols or in the presence of a range of anions or of common oxidants was checked. Fig. S19 shows the obtained results. For all competitor species investigated we observed a quenching of the initial fluorescence intensity of complex **1** with the exception of NO_x^-, alanine and cysteine for which a modest raise in the fluorescence response was observed. This finding suggests a good selectivity of our probe for HS^- under the experimental conditions tested.

Next, we checked the reversibility of HS^- binding to the systems under investigation, by analogy with sensing constructs set up by us and others in the past [55,56]. To test the reversibility of HS^- binding to complex **1**, we prepared the complex **1**-HS species *in situ* by adding 5 equiv of NaSH to the complex in DMSO followed by an excess of acetic acid. The initial fluorescence intensity of complex **1**, which enhances upon the addition of HS^- (as already seen in the fluorescence scan experiment in Fig. 3), was quenched when acetic acid was added (i.e. HS^- coordination is acid-labile, thus allowing for chemically reversible coordination of HS^- by the addition of a suitable proton source: see Scheme 1). Fig. S20 shows a typical time trace of a solution containing 10 μM of complex **1** when excited at 445 nm. This finding provides evidence of the stability of complex **1** during the time-dependent fluorescence experiment.

The limit of detection (LOD) of complex **1** for HS^- was found to be 0.43 μM (Fig. S21 and Table S1 in the SI).

To further advance our understanding of the coordination properties of the compounds under investigation with HS^- and their photophysical properties we performed a computational analysis at the density functional theory (DFT) level (see experimental section for more details). Minimum energy geometries of the molecules and of their HS^- adducts (also considering the possibility of multiple adducts) have been computed both for the ground state and for the first excited singlet state. The computed ground state optimum geometries of HS^- complexes are shown in Fig. 4.

The formation of the single adduct for all the complexes is predicted to be exoergonic ($\Delta E = -0.88$ eV for **1**, $\Delta E = -0.83$ eV for **2**, $\Delta E = -0.20$ eV for **3** and $\Delta E = -0.30$ eV for **4**). For complex **3** we have also studied the possible formation of HS^- adducts through coordination of HS^- to the Zn atom and the expulsion of the two Cl^- ions. All the adducts are predicted to be stable, and the most stable one is obtained through the expulsion of both Cl^- ions ($\Delta E = -0.64$ eV, reported in Fig. 4). This finding corroborates what is observed by NMR experiments (Fig. S13).

Our DFT study also allowed rationalizing the experimentally observed change in fluorescence intensity after the coordination of HS^- for complexes **1** and **2**. In particular, our predictions show that emission from the first excited electronic state (S_1) are electric dipole allowed transitions for all the species under study; therefore, the enhancement of fluorescence for complex **1** and the quenching of fluorescence observed for complex **2** after the coordination of HS^- has to be related with the

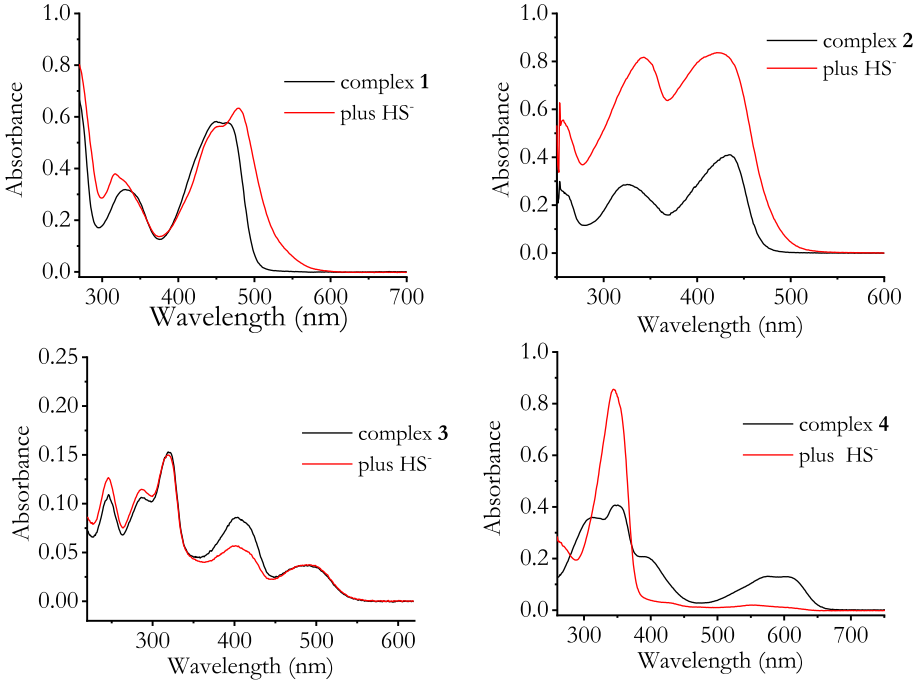


Fig. 2. Electronic absorption spectra of complexes **1**–**4** before and after the addition of 50 μM of NaSH. [Complexes] = 1×10^{-5} M, spectra recorded in DMSO for complexes **1** and **2**, in MeOH for **3** and **4**.

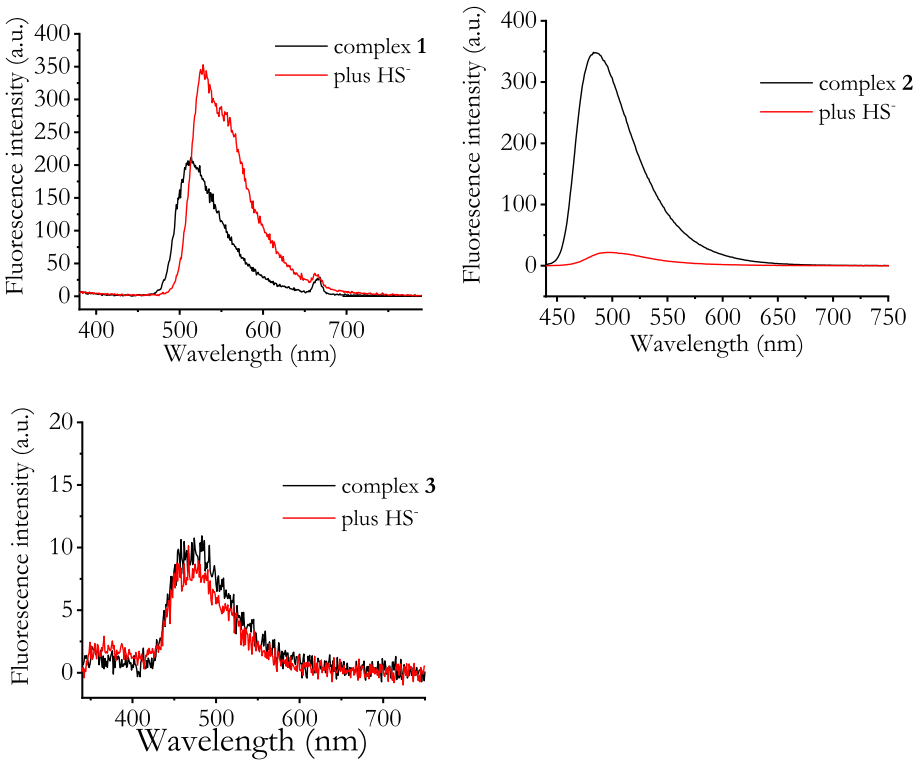
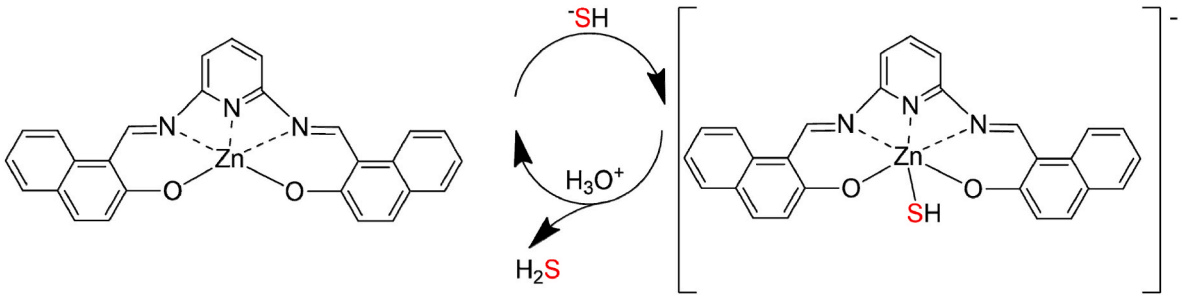


Fig. 3. Emission spectra of complexes **1**–**3** before and after the addition of 3 equivalents of NaSH. [Complexes] = 5×10^{-6} M. Spectra were measured in DMSO with λ_{exc} = 442 nm for complex **1**; λ_{exc} = 434 nm for complex **2**; in MeOH with λ_{exc} = 320 nm for complex **3**.



Scheme 1. Binding mechanism of HS^- to complex **1**.

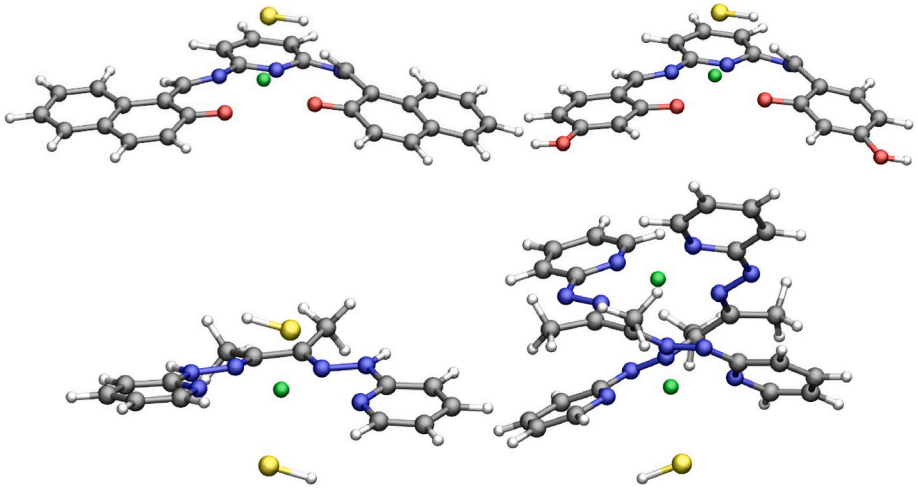


Fig. 4. Optimized geometry for the adduct with HS^- of **1** (top left), **2** (top right),**3** (bottom left) and **4** (bottom right).

possible existence of non-radiative decay paths. We have thus investigated the energy location of the lowest triplet states, which could be responsible for the different fluorescence quantum yields of complex **1** and complex **2** and their HS^- adducts (Table 1).

The energies of the four lowest triplet states are reported in Fig. 5; T_4 lies always above in energy than S_1 and therefore it should not be involved in non-radiative decay paths. Inspection of Fig. 5 shows that the triplet states closer in energy to S_1 change significantly after the coordination with HS^-; however, based on the energy gap rule, most important decay path should involve the triplet states nearest in energy to S_1.

For both complexes, we see that the $S_1 \rightarrow T_x$ (T_x being the nearest triplet states with energy lower than S_1) transition is exoergonic both before and after coordination; however, while for complex **2** that transition is more favoured after HS^- coordination, as demonstrated by the lower energy difference between S_1 and the nearest triplet state (Fig. 5) and by the significantly higher spin-orbit coupling for S_1 and the nearest triplet state (see Table 1), exactly the opposite occurs for complex **1**. Thus, while an enhancement is expected for complex **1** after coordination of HS^-, a quenching of fluorescence is to be expected for complex **2** in the presence of HS^-, as was indeed experimentally observed (see Fig. 3).

With these results in our hands, and inspired by the encouraging results obtained by immobilizing salen complexes in sulfonated PPO films [12] we also thought of entrapping complex **1** (the most promising of the family of complexes under investigation in this work) in a polymer shell, this time choosing biocompatible polymer films (e.g. PBS). Further than reusability and stability, biocompatible polymers offer the advantage of applications in biological media which is a key improvement in practical measurements. PBS films have been prepared by casting procedures as described in the experimental section and characterized by X-ray diffraction measurements.

In Fig. 6, X-ray diffraction profile of a PBS film prepared by casting at 60 °C is shown. The strongest diffraction peaks corresponding to the (020), (110), and (111) planes of the poly(butylene)succinate monoclinic crystal lattice, are clearly visible [57,58].

The degree of crystallinity (x_c) was calculated using the following equation:

$$x_c = \frac{A_c}{(A_a + A_c)}$$

where A_c and A_a are the integrated areas calculated under the crystalline phase and amorphous phase respectively.

The degree of crystallinity (x_c) for the reported PBS film is nearly 33 %.

The fluorescence intensity of complex **1** absorbed in PBS film, with the film immersed in water solution, was monitored as a function of time during the change from a HS^- rich to a HS^- free environment and vice versa. Fig. 7 displays the results: a cyclable fluorescence response was recorded. Cycles were started by adding HS^- (i.e., in considerable excess over the complex concentration) and completed by adding a few drops of acetic acid to the solution surrounding the film for the removal of H_2S. A fast enhancement in fluorescence emission was clearly observed upon each HS^- addition. When adding acetic acid to displace the HS^-, the fluorescence intensity returned to the initial level; the cycle has been repeated 5 times.

Table 1
Spin-Orbit coupling elements (cm^{-1}) for complex **1**, complex **2** and their adducts, evaluated at the S_1 geometry.

	SOC T_1-S_1	SOC T_2-S_1	SOC T_3-S_1
1	7.64	11.96	8.77
1 + HS^-	1.25	6.88	2.77
2	1.68	15.58	7.17
2 + HS^-	98.95	43.44	16.39

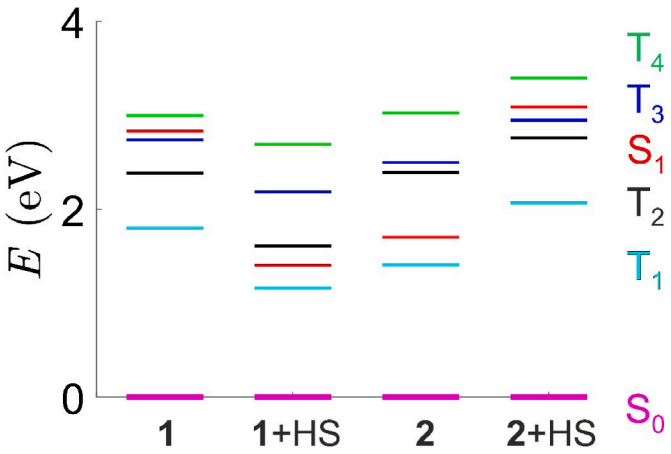


Fig. 5. Computed energies (E, eV) of the ground state (S_0) first excited singlet (S_1), and four lowest energy triplet states, evaluated at the S_1 geometry for complex **1**, complex **2**, and their HS^-adducts.

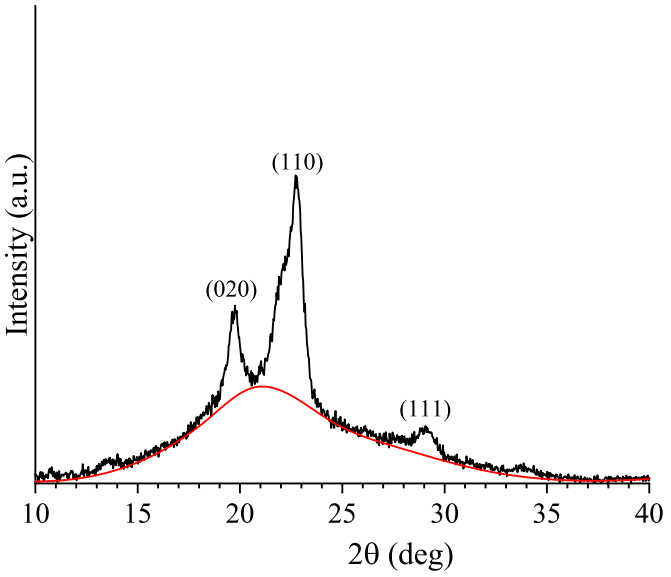


Fig. 6. WAXD pattern of the PBS film.

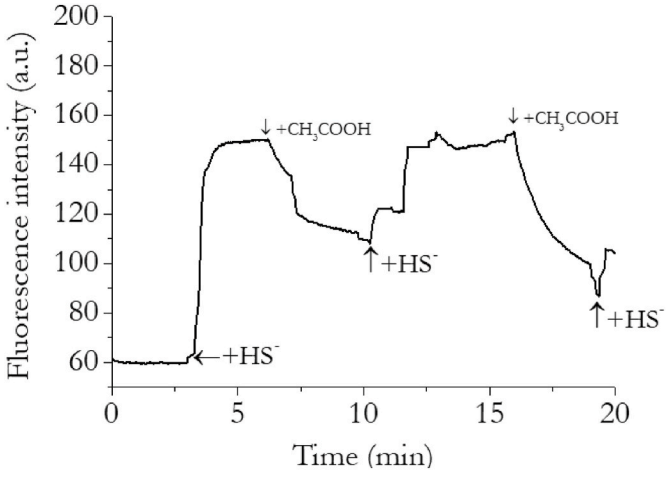


Fig. 7. Fluorescence intensity time trace observed at 550 nm (exc 470 nm) of PBS doped with complex **1** upon addition and removal of HS^-. [HS^-] = 3 mM; [CH_3COOH] = 1 wt%. NaSH and CH_3COOH dissolved in water.

These findings showed that the HS^- binding process is reversible even when the complex is sorbed in PBS films, and that the fluorescence response is retained also when the sensing device is in the solid state: both conditions are crucial for practical sensing applications. Upon storage of the PBS-sorbed films at room temperature the usability/durability of the sensing films, was found to be at least of one week.

In an effort to assess if there is a dependence of the fluorescence intensities on the HS^- concentration we performed a series of measurements with increased concentrations of NaSH. Fig. S22 displays the results: as clearly visible fluorescence intensities depend on [HS^-], in agreement with what we observed for the solution experiments (Fig. S18).

3. Conclusions

The present study provides evidence that linking pyridines with other π-conjugated motifs has significant potential for developing a new class of small-molecule fluorophores which can be successfully applied in the field of H_2S sensing. In addition, the sortpion of the fluorescent sensing molecules in a biocompatible and biodegradable polymer film offers advantages in terms of reusability and robustness of the implemented device and opens the door to new kinds of applications within biological environments. We foresee that these findings can trigger new ideas for applications beyond the field of H_2S sensing.

4. Experimental section

4.1. Materials

All chemicals used for the synthetic work were obtained from Sigma-Aldrich and were of reagent grade. They were used without further purification. Syntheses of ligands [59–61] and complexes [42,43,51,52] were performed by following literature procedures.

4.2. General

HR MALDI mass spectra were recorded using a Bruker solariX XR Fourier transform ion cyclotron resonance (FT-ICR) mass spectrometer (Bruker Daltonik GmbH, Bremen, Germany) equipped with a 7 T refrigerated actively-shielded superconducting magnet (Bruker Biospin, Wissembourg, France). The samples were ionized in positive or negative ion mode using the MALDI ion source. The mass range was set to *m/z* 150–2000. The laser power was 15 % and 15 laser shots were used for each scan. Mass spectra were calibrated externally using a mix of peptide clusters in MALDI ionization positive ion mode. A linear calibration was applied. NMR spectra were recorded on a Bruker AVANCE 400 NMR instrument (^{1}H NMR, 400.13 MHz; ^{13}C NMR, 100.62 MHz) or on a 600 MHz spectrometer [600 (^{1}H NMR) and 150 MHz (^{13}C NMR)] using 5 mm o.d. NMR tubes. Typically, 5 mg of the complex in 0.5 mL of the solvent were used for each experiment.

Fourier transform infrared (FTIR) spectra were collected in the range 4000-400 cm^{-1} with a resolution of 2.0 cm^{-1} by using a Vertex 70 Bruker spectrometer, equipped with a DTGS detector and a Ge/KBr beam splitter. To increase the signal-to-noise ratio, thirty-two scans were averaged.

4.3. Synthesis and characterization of complex 1

To a stirred solution containing the ligand precursor [1,1'-((1E,1′E)-(pyridine-2,6-diylbis(azaneylylidene))bis(methaneylylidene))bis(naphthalen-2-ol)] (0.219 g, 0.5 mmol) in dry benzene (4.0 mL) was added dropwise a solution of $ZnEt_2$ (0.065 g, 0.5 mmol) in dry benzene (1.5 mL) under a nitrogen atmosphere, then the solution was stirred overnight at room temperature. The solvent was removed under vacuum, forming an orange solid. The formation of the desired species was confirmed by NMR analysis. Yield: 90 %.

MS (MALDI FT-ICR, $CHCl_3$): *m/z* (%) calculated: 961.1453 experimental: 961.1487 ([complex **1**]$^+$)$_2$; calculated: 481.5802 experimental: 481.5702 ([complex **1**]$^+$). **^{1}H NMR (400 MHz, DMSO-d_6, 298 K):** 9.46 (s, 2H, CH═N), 7.77 (d, J = 8,66 Hz, 2H, $H_{aromatic}$), 7.48-7.32 (m, 8H, $H_{aromatic}$), 6.93 (d, J = 7,97 Hz, 2H, $H_{aromatic}$), 6.81 (d, J = 9,70 Hz, 2H, $H_{aromatic}$).

Emission (DMSO, λ_{exc} = 440 nm), λ_{max}, nm (quantum yield, Φ_F): 500 nm (0.2); λ_f^{max} = 514,02 nm, λ_a^{max} = 449,95 nm, Stokes shift (Δλ) = 64,06 nm.

4.4. Synthesis and characterization of complex 2

To a stirred solution containing 2,4-dihydroxybenzaldehyde (0.276 g, 0.002 mmol) in absolute ethanol (50.0 mL) was added 2,6-diaminopyridine (0.109 g, 0.001 mmol), then the solution was stirred for 1h at room temperature. After 1 h the reaction mixture was added to a stirred solution of $Zn(CH_3COO)_2$ (0.219 g, 0.001 mmol) in absolute ethanol (150.0 mL), then the reaction was stirred overnight under reflux. The solvent was removed under vacuum, forming a dark-yellow solid. The formation of the desired species was confirmed by NMR analysis. Yield: 83 %.

MS (MALDI FT-ICR, solid sample): *m/z* (%) calculated: 823.0467 experimental: 823.0643 ([complex **2**]$^+$; calculated: 845.0287 experimental: 845.0545 ([complex **2**]Na^+. **^{1}H NMR (400 MHz, DMSO-d_6, 298 K)**: 9.15 (s, 2H, CH═N), 7.11-7.05 (m, 3H, $H_{aromatic}$), 6.08 (d, J = 2,24 Hz, 4H, $H_{aromatic}$), 5.56 (d, J = 8,53 Hz, 2H, $H_{aromatic}$).

Emission (DMSO, λ_{exc} = 435 nm), λ_{max}, nm (quantum yield, Φ_F): 500 nm (0.3); λ_f^{max} = 484,92 nm, λ_a^{max} = 434,93 nm, Stokes shift (Δλ) = 49,99 nm.

4.5. Synthesis and characterization of complex 3

To a stirred solution containing the ligand precursor [2,2'-(((2E,3E)-butane-2,3-diylidene)bis(hydrazin-1-yl-2-ylidene))dipyridine] (0.185 g, 0.689 mmol) in absolute ethanol (20.0 mL) was added dropwise a solution of $ZnCl_2$ (0.110 g, 0.807 mmol) in absolute ethanol (5.0 mL) under a nitrogen atmosphere, then the solution was stirred for 3 h under reflux. Then the mixture was filtered, a dark-yellow solid was obtained and washed with cold methanol. The formation of the desired species was confirmed by NMR analysis. Yield: 87 %.

MS (MALDI FT-ICR, MeOH): *m/z* (%) calculated: 404.0203 experimental: 403.9925 ([complex **3**]$^+$. **^{1}H NMR (400 MHz, DMSO-d_6, 298 K)**: 9.81 (s, 1H, CH═N), 8.16 (s, 1H, $H_{aromatic}$), 7.67 (t, J = 7,41 Hz, 1H, $H_{aromatic}$), 7.24 (d, J = 8,37 Hz, 1H, $H_{aromatic}$), 6.82 (d, J = 6,13 Hz, 1H, $H_{aromatic}$), 2.22 (s, 3H, CH_3).

Emission (DMSO, λ_{exc} = 320 nm), λ_{max}, nm (quantum yield, Φ_F): 480 nm (0.08); λ_f^{max} = 474,00 nm, λ_a^{max} = 319,01 nm, Stokes shift (Δλ) = 154,98 nm.

4.6. Synthesis and characterization of complex 4

To a stirred solution containing the ligand precursor [2,2'-(((2E,3E)-butane-2,3-diylidene)bis(hydrazin-1-yl-2-ylidene))dipyridine] (0.141 g, 0.5 mmol) in dry THF (5.0 mL) was added dropwise a solution of $ZnEt_2$ (0.065 g, 0.5 mmol) in dry THF (5.0 mL) under a nitrogen atmosphere, then the solution was stirred overnight at room temperature. The solvent was removed under vacuum, forming a dark-yellow solid. The formation of the desired species was confirmed by NMR analysis. Yield: 78 %.

MS (MALDI FT-ICR, MeOH): *m/z* (%) calculated: 661.1215 experimental: 661.1244 ([complex **4**]$^+$. **^{1}H NMR (400 MHz, DMSO-d_6, 298 K)**: 7.70 (s, 1H, $H_{aromatic}$), 7.13 (m, 1H, $H_{aromatic}$), 6.43 (m, 1H, $H_{aromatic}$), 6.09 (m, 1H, $H_{aromatic}$), 2.06 (s, 3H, CH_3).

Absorbance and fluorescence measurements. Absorption spectra were recorded on a Cary-50 Spectrophotometer, using a 1 cm quartz cuvette (Hellma Benelux bv, Rijswijk, Netherlands) and a slit-width equivalent to a bandwidth of 5 nm. Fluorescence spectra were

measured on a Cary Eclipse Spectrophotometer in a 10 × 10 mm^2 airtight quartz fluorescence cuvette (Hellma Benelux bv, Rijswijk, Netherlands) with an emission band-pass of 10 nm and an excitation band-pass of 5 nm. Both absorption and fluorescence measurements were performed either in DMSO or in Milliq water solutions at 25 °C. Fluorescence emission spectra were registered by exciting the samples at a specific wavelength (as stated in the figure captions).

Fluorescence quantum yield (Φ_F) values were measured in optically diluted solutions using as standards the commercial dyes Cy3 NHS (Φ_F = 0.15 in MilliQ water), according to the equation [62].

$$\Phi_F^s = \Phi_F^r (I_s/I_r)(A_r/A_s)(\eta_s/\eta_r)$$ [2].

where indexes s and r denote the sample and reference, respectively. *I* stands for the integrated emission intensity, *A* is the absorbance at the excitation wavelength, and η is the refractive index of the solvent. The optical density of complexes and standards was kept below 0.1. The uncertainty in the determination of Φ_F is ±15 %.

Calculation of the limit of detection (LOD). In agreement with the IUPAC recommendation [63,64], the limit of detection for HS^- was calculated from the spectrofluorometric titration data, for complex **1**, using the following equation:

$$LOD = 3\ s/K$$

where s and K represent, respectively, the standard deviation of the blank and the absolute value of the slope of the calibration line (Fig. S21). All data involved in the calculation of LOD are reported in Fig. S21 and Table S1.

NMR characterization of the complexes upon addition of HS^-. The NMR tube was charged with the free complex solutions in DMSO-d_6 then NaSH solid or in solution (to the end concentrations specified in the figure captions) was added and the spectra registered.

Preparation of PBS films. PBS films were prepared by casting procedures, dissolving 0.5 g of polymer in 10 mL of chloroform at 120°, subsequently, the solution was poured into a Petri dish at 60 °C, until complete solvent evaporation.

Characterization of PBS films. Wide-angle X-ray diffraction (WAXD) patterns were collected by using a D2 QUEST Bruker diffractometer with nickel-filtered Cu Kα radiation.

Adsorption of complex 1 in PBS films. PBS films were immersed in a saturated complex/acetone solution (~1.0 wt%) for 1 min at room temperature. Then the PBS films were dried by thermal treatment at 60 °C for 30 min.

Computational details. All electronic computations have been carried out at the density functional level of theory using the range separated hybrid functional CAM-B3LYP with TZVP basis set as implemented in the Gaussian package (G16) [65]. That combination of functional and basis set has been chosen because it leads to accurate predictions, as discussed in previous works [66,67]. Effects due to solvent (DMSO) polarization were included by the polarizable continuum model (PCM) [68].

CRediT authorship contribution statement

Alessio Trerotola: Investigation, Data curation. **Paola Rizzo:** Supervision, Data curation. **Angela Erbaggio:** Investigation. **Viktoriia Vykhovanets:** Investigation, Data curation. **Alessandro Landi:** Investigation. **Marina Lamberti:** Data curation. **Carmine di Fiore:** Investigation. **Claudio Pellecchia:** Funding acquisition. **Maria Strianese:** Writing – original draft, Formal analysis, Conceptualization.

Declaration of competing interest

Authors declare no conflict of interest.

Acknowledgments

We acknowledge financial support under the National Recovery and Resilience Plan (NRRP), Mission 4, Component 2, Investment 1.1, Call for tender **No. 1409 published on 14.9.2022** by the Italian Ministry of University and Research (MUR), funded by the European Union – NextGenerationEU– Project Title: "*A bottom/up approach for the study of the crystal structure of sustainable and eco-friendly polymers and the relationships with properties – ECOPOLYCRYS*" – CUP **E53D23015900001** – Grant Assignment Decree No. **1384 adopted on 1/09/2023** by the Italian Ministry of Ministry of University and Research (MUR).

Appendix A. Supplementary data

Supplementary data to this article can be found online at https://doi.org/10.1016/j.dyepig.2025.112786.

Data availability

Data will be made available on request.

References

[1] Wang P, Zhang G, Wondimu T, Ross B, Wang R. Hydrogen sulfide and asthma. Exp Physiol 2011;96:847–52. https://doi.org/10.1113/expphysiol.2011.057448.
[2] Whiteman M, Le-áTrionnaire S, Chopra M, Fox B, Whatmore J. Emerging role of hydrogen sulfide in health and disease: critical appraisal of biomarkers and pharmacological tools. Clin Sci 2011;121:459–88. https://doi.org/10.1042/CS20110267.
[3] Kimura H. Signaling molecules: hydrogen sulfide and polysulfide. Antioxid Redox Signaling 2014;22:362–76. https://doi.org/10.1089/ars.2014.5869.
[4] Davis AG, Zakharov LN, Pluth MD. Reversible hydrosulfide (HS^-) binding using exclusively C−H hydrogen-bonding interactions in imidazolium hosts. Inorg Chem 2024;63:3057–62. https://doi.org/10.1021/acs.inorgchem.3c03922.
[5] Fosnacht KG, Hammers MD, Earp MS, Gilbert AK, Pluth MD. A cell trappable methyl Rhodol-based fluorescent probe for hydrogen sulfide detection. Chem Asian J 2022;17:e202200426. https://doi.org/10.1002/asia.202200426.
[6] Pluth MD, Tonzetich ZJ. Hydrosulfide complexes of the transition elements: diverse roles in bioinorganic, cluster, coordination, and organometallic chemistry. Chem Soc Rev 2020;49:4070–134. https://doi.org/10.1039/C9CS00570F.
[7] Smith HM, Pluth MD. Advances and opportunities in H_2S measurement in chemical biology. JACS Au 2023;3:2677–91. https://doi.org/10.1021/jacsau.3c00427.
[8] Fosnacht KG, Pluth MD. Activity-based fluorescent probes for hydrogen sulfide and related reactive sulfur species. Chem. Rev. 2024;124:4124–257. https://doi.org/10.1021/acs.chemrev.3c00683.
[9] Strianese M, Pappalardo D, Mazzeo M, Lamberti M, Pellecchia C. The contribution of metalloporphyrin complexes in molecular sensing and in sustainable polymerization processes: a new and unique perspective. Dalton Trans. 2021;50:7898–916. https://doi.org/10.1039/D1DT00841B.
[10] Lu K, Wang Y, Wang C, Liu R, Yang K, Zhang X, Xiao H. A bioluminescent probe for H_2S detection in tumor microenvironment. ACS Bio Med Chem Au 2025;5:175–83. https://doi.org/10.1021/acsbiomedchemau.4c00102.
[11] Strianese M, Palm GJ, Kohlhause D, Ndamba LA, Tabares LC, Pellecchia C. Azurin and HS−: towards implementation of a sensor for HS^- detection. Eur J Inorg Chem 2019;2019:885–91. https://doi.org/10.1002/ejic.201801399.
[12] Rizzo P, Cozzolino A, Syed S, Vykhovanets V, Landi A, Pietro Oliveri I, Pellecchia C, Strianese M. A fluorescently-doped thermoplastic polymer as a proof-of-principle device for the detection and capture of H_2S and its HS^- anion. J Photochem Photobiol, A: Chem 2025;458:115993–6002. https://doi.org/10.3390/s23042023.
[13] Wang KN, Liu LY, Mao D, Xu S, Tan CP, Cao Q, Mao ZW, Liu B. A polarity-sensitive ratiometric fluorescence probe for monitoring changes in lipid droplets and nucleus during ferroptosis. Angew Chem Int Ed 2021;60:15095–100. https://doi.org/10.1002/anie.202104163.
[14] Li X, Long C, Cui Y, Tao F, Yu X, Lin W. Charge-dependent strategy enables a single fluorescent probe to study the interaction relationship between mitochondria and lipid droplets. ACS Sens 2021;6:1595–603. https://doi.org/10.1021/acssensors.0c02677.
[15] Kaur M, Choi DH. Diketopyrrolopyrrole: brilliant red pigment dye-based fluorescent probes and their applications. Chem Soc Rev 2015;44:58–77. https://doi.org/10.1039/C4CS00248B.
[16] Martinez V, Henary M. Nile red and nile blue: applications and syntheses of structural analogues. Chem Eur J 2016;22:13764–82. https://doi.org/10.1002/chem.201601570.
[17] Kolemen S, Akkaya EU. Reaction-based BODIPY probes for selective bio-imaging. Coord Chem Rev 2018;354:121–34. https://doi.org/10.1016/j.ccr.2017.06.021.
[18] Liu X, Lu X, Zhu T, Wenli D, Zhenghui Y, Cao H, Wang S, Tian Y, Zhang Z, Zhang R, De Souza SC, Tian X. Revealing lipid droplets evolution at nanoscale under

proteohormone stimulation by a BODIPY- hexylcarbazole derivative. Biosens Bioelectron 2021;175:112871. https://doi.org/10.1016/j.bios.2020.112871.
[19] Hu Y, Li X, Fang Y, Shi W, Li X, Chen W, Xian M, Ma H. Reactive oxygen species-triggered off-on fluorescence donor for imaging hydrogen sulfide delivery in living cells. Chem Sci 2019;10:7690–4. https://doi.org/10.1039/C9SC02323B.
[20] Chen J, Wang C, Liu W, Qiao Q, Qi H, Zhou W, Xu N, Li J, Piao H, Tan D, Liu X, Xu Z. Stable super-resolution imaging of lipid droplet dynamics through a buffer strategy with a hydrogen-bond sensitive fluorogenic probe. Angew Chem Int Ed 2021;60:25104–13. https://doi.org/10.1002/anie.202111052.
[21] Mota AAR, Correa JR, de Andrade LP, De Souza Cintra GA, Freitas-Junior LH, da Silva WA, de Oliveira HCB, Neto BAD. From live cells to Caenorhabditis elegans: selective staining and quantification of lipid structures using a fluorescent hybrid benzothiadiazole derivative. ACS Omega 2018;3:3874–81. https://doi.org/10.1021/acsomega.8b00434.
[22] Medeiros IR, Barbosa ALA, Balaguez RA, Lopes TO, de Oliveira HCB, Alves D, Neto BAD. Fluorescent benzoselenadiazoles: synthesis, characterization, and quantification of intracellular lipid droplets and multicellular model staining. J Org Chem 2020;85:10561–73. https://doi.org/10.1021/acs.joc.0c01031.
[23] Tatenaka Y, Kato H, Ishiyama M, Sasamoto K, Shiga M, Nishitoh H, Ueno Y. Monitoring lipid droplet dynamics in living cells by using fluorescent probes. Biochemistry 2019;58:499–503. https://doi.org/10.1021/acs.biochem.8b01071.
[24] Zhou R, Wang C, Liang X, Liu F, Yan X, Liu X, Sun P, Zhang H, Wang Y, Lu G. Stimulated emission depletion (STED) super-resolution imaging with an advanced organic fluorescent probe: visualizing the cellular lipid droplets at the unprecedented nanoscale resolution. ACS Mater Lett 2021;3:516–24. https://doi.org/10.1021/acsmaterialslett.1c00143.
[25] Feckovà M, le Poul P, Guen FR, Roisnel T, Pytela O, Klikar M, Bures F, Achelle S. 2,4-Distyryl- and 2,4,6-tristyrylpyrimidines: synthesis and photophysical properties. J Org Chem 2018;83:11712–26. https://doi.org/10.1021/acs.joc.8b01653.
[26] Hu R, Chen B, Wang Z, Qin A, Zhao Z, Lou X, Tang BZ. Intriguing chameleon fluorescent bioprobes for the visualization of lipid droplet-lysosome interplay. Biomaterials 2019;203:43–51. https://doi.org/10.1016/j.biomaterials.2019.03.002.
[27] Tan P, Zhuang W, Li S, Zhang J, Xu H, Yang L, Liao Y, Chen M, Wei Q. A lipid droplet targeted fluorescent probe for high-efficiency image-guided photodynamic therapy of renal cell carcinoma. Chem. Commun. 2021;57:1046–9. https://doi.org/10.1039/D0CC07336A.
[28] Zhao N, Li Y, Yang W, Zhuang J, Li Y, Li N. Multifunctional pyrazoline based AIEgens: real-time tracking and specific protein fishing of lipid droplets. Chem Sci 2019;10:9009–16. https://doi.org/10.1039/C9SC03111A.
[29] Taki M, Kajiwara K, Yamaguchi E, Sato Y, Yamaguchi S. Fused thiophene-S,S-dioxide-Based super-photostable fluorescent marker for lipid droplets. ACS Mater Lett 2021;3:42–9. https://doi.org/10.1021/acsmaterialslett.0c00451.
[30] Liu G, Peng G, Dai J, Zhou R, Wang C, Yan X, Jia X, Liu X, Gao Y, Wang L, Lu G. STED nanoscopy imaging of cellular lipid droplets employing a superior organic fluorescent probe. Anal Chem 2021;93:14784–91. https://doi.org/10.1021/acs.analchem.1c03474.
[31] Tydlitát J, Achelle S, Rodriguez-Lopez J, Pytela O, Mikysek T, Cabon N, Robin-le Guen F, Miklik D, Rezickova Z, Bures F. Photophysical properties of acid-responsive triphenylamine derivatives bearing pyridine fragments: towards white light emission. Dyes Pigments 2017;146:467–78. https://doi.org/10.1016/j.dyepig.2017.07.043.
[32] Achelle S, Verbitskiy EV, Feckovà M, Bures F, Barsella A, Robin-le Guen F. V-shaped methylpyrimidinium chromophores for nonlinear optics. ChemPlusChem 2021;86:758–62. https://doi.org/10.1002/cplu.202100081.
[33] Yang W, Luo D, Li G, Luo Q, Banwell MG, Chen L. Synthesis of pyridin-1(2H)-ylacrylates and the effects of different functional groups on their fluorescence. Molecules 2023;28. https://doi.org/10.3390/molecules28186511.
[34] Strianese M, Brenna S, Ardizzoia G, Guarnieri D, Lamberti M, D'Auria I, Pellecchia C. Imidazo-pyridine-based zinc(ii) complexes as fluorescent hydrogen sulfide probes. Dalton Trans 2021;50:17075–85. https://doi.org/10.1039/D1DT02489B.
[35] Consiglio G, Oliveri IP, Cacciola S, Maccarrone G, Failla S, Di Bella S. Dinuclear zinc(ii) salen-type Schiff-base complexes as molecular tweezers. Dalton Trans. 2020;49:5121–33. https://doi.org/10.1039/D0DT00494D.
[36] Di Bella S. Lewis acidic zinc(ii) salen-type Schiff-base complexes: sensing properties and responsive nanostructures. Dalton Trans 2021;50:6050–63. https://doi.org/10.1039/D1DT00949D.
[37] Oliveri IP, Di Bella S. Lewis acidic zinc(II) complexes of tetradentate ligands as building blocks for responsive assembled supramolecular structures. Chemistry 2023;5:119–37. https://doi.org/10.3390/chemistry5010010.
[38] Kleij AW, Kuil M, Tooke DM, Lutz M, Spek AL, Reek JNH. Zn(II)-Salphen complexes as versatile building blocks for the construction of supramolecular box assemblies. Chem Eur J 2005;11:4743–50. https://doi.org/10.1002/chem.200500227.
[39] Lamberti M, Galotto MV, Vasca E, Landi A, Peluso A, Strianese M. Effect of metal coordination environment on the stability of zinc complexes and their reactivity with NaSH. ChemistrySelect 2024;9:e202401334. https://doi.org/10.1002/slct.202401334.
[40] Strianese M, D'Auria GJ, Lamberti M, Landi A, Peluso A, Varriale A, D'Auria S, Pellecchia C. Salen, salan and salalen zinc(ii) complexes in the interaction with HS−: time-resolved fluorescence applications. Dalton Trans. 2023;52:1357–65. https://doi.org/10.1039/D2DT03730K.
[41] Strianese M, Lamberti M, Persico A, Pellecchia C. Reactivity of monohydrogensulfide with a suite of pyridoxal-based complexes: a combined NMR, ESI-MS, UV−visible and fluorescence study. Inorg Chim Acta 2020;501:119235. https://doi.org/10.3390/s22093173.
[42] Strianese M, Ferrara G, Vykhovanets V, Blal N, Guarnieri D, Landi A, Lamberti M, Peluso A, Pellecchia C. Sol-gel dipping devices for H_2S visualization. Sensors 2023;23:2023–37. https://doi.org/10.3390/s23042023.
[43] Strianese M, Vykhovanets V, Blal N, Guarnieri D, Landi A, Lamberti M, Peluso A, Pellecchia C. Paper-strip-based sensors for H_2S detection: a proof-of-principle study. Sensors 2022;22:3173–86. https://doi.org/10.3390/s22093173.
[44] Rombach M, Vahrenkamp H. Pyrazolylborate−Hydrosulfide complexes and their reactions. Inorg Chem 2001;40:144–6150. https://doi.org/10.1021/ic010510+.
[45] Aliotta L, Seggiani M, Lazzeri A, Gigante V, Cinelli P. A brief review of poly (butylene succinate) (PBS) and its main copolymers: synthesis, blends, composites. Biodegradability, and Applications 2022;14. https://doi.org/10.3390/polym14040844.
[46] Nelson TF, Baumgartner R, Jaggi M, Bernasconi SM, Battagliarin G, Sinkel C, Kunkel A, Kohler HP, McNeill K, Sander M. Biodegradation of poly(butylene succinate) in soil laboratory incubations assessed by stable carbon isotope labelling. Nature Commun 2022;13:5691–707. https://doi.org/10.1038/s41467-022-33064-8.
[47] Barletta M, Aversa C, Ayyoob M, Gisario A, Hamad K, Mehrpouya M, Vahabi H. Poly(butylene succinate) (PBS): materials, processing, and industrial applications. Prog Polym Sci 2022;132:101579. https://doi.org/10.1016/j.progpolymsci.2022.101579.
[48] Gigli M, Fabbri M, Lotti N, Gamberini R, Rimini B, Munari A. Poly(butylene succinate)-based polyesters for biomedical applications: a review. Eur Pol J 2016;75:431–60. https://doi.org/10.1016/j.eurpolymj.2016.01.016.
[49] Mtibe A, Muniyasamy S, Teboho M, Ofosu O, Ojijo V, John M. Recent insight into the biomedical applications of polybutylene succinate and polybutylene succinate-based materials. Express Polym Lett 2023;17(2023.2):2–28. https://doi.org/10.3144/expresspolymlett.
[50] Hsieh HC, Wu N, Chuang TH, Lee WY, Chen JY, Chen WC. Eco-friendly polyfluorene/poly(butylene succinate) blends and their electronic device application on biodegradable substrates. ACS Appl Polym Mater 2020;2:2469–76. https://doi.org/10.1021/acsapm.0c00439.
[51] Pandiarajan D, Fox T, Spingler B. An N4-tetradentate hydrazone ligand that binds in a neutral, mono- and bisdeprotonated form to iron(II) and zinc(II) metal ions. Crystals 2021;11:982–94. https://doi.org/10.3390/cryst11080982.
[52] Milione S, Capacchione C, Cuomo C, Strianese M, Bertolasi V, Grassi A. New zinc complexes bearing k2-heteroscorpionate ligands: influence of second-sphere bonding interactions on reactivity and properties. Inorg Chem 2009;48:9510–8. https://doi.org/10.1021/ic901091e.
[53] Rombach M, Vahrenkamp H. Pyrazolylborate-zinc-hydrosulfide complexes and their reactions. Inorg Chem 2001;40:6144–50. https://doi.org/10.1021/ic010510+.
[54] Galardon E, Tomas A, Selkti M, Roussel P, Artaud I. Synthesis, characterization, and reactivity of alkyldisulfanido zinc complexes. Inorg Chem 2009;48:5921–7. 0.1021/ic900238v.
[55] Strianese M, Pellecchia C. Fluorescent probes for H_2S detection: metal-based approaches. In: Hydrogen sulfide; 2022. p. 203–33. https://doi.org/10.1002/9781119799900.ch9.
[56] Hartle MD, Sommer SK, Dietrich SR, Pluth MD. Chemically reversible reactions of hydrogen sulfide with metal phthalocyanines. Inorg Chem 2014;53:7800–2. https://doi.org/10.1021/ic500664c.
[57] Wang K, Jiao T, Wang Y, Li M, Li Q, Shen C. The microstructures of extrusion cast biodegradable poly(butylene succinate) films investigated by X-ray diffraction. Mater Lett 2013;92:334–7. https://doi.org/10.1016/j.matlet.2012.10.121.
[58] Righetti MC, Di Lorenzo ML, Cavallo D, Muller AJ, Gazzano M. Structural evolution of poly(butylene succinate) crystals on heating with the formation of a dual lamellar population, as monitored by temperature-dependent WAXS/SAXS analysis. Polymer 2023;268:125711. https://doi.org/10.1016/j.polymer.2023.125711.
[59] Saberyan K, Zolfonoun E, Shamsipur M, Salavati-Niasari M. Amberlite XAD-4 Impregnated with a new pentadentate schiff-base: a chelating collector for separation and preconcentration of trace amounts of Gallium (III) and Indium (III). Acta Chim Slov 2010;57:222–9.
[60] Guhathakurta B, Biswas C, Naskar JP, Lu L, Zhu M. Synthesis and crystal structure of [Cu(BDBPH)(ClO4)2] (BDBPH = butane-2,3-dione bis(2-pyridylhydrazone). J Chem Crystallogr 2011;41:1694–9. https://doi.org/10.1007/s10870-011-0159-7.
[61] Strianese M, Lamberti M, Mazzeo M, Pellecchia C. A comparative study on the polymerization of α-olefins catalyzed by salen and salan Zirconium complexes. Macromol Chem Phys 2008;209:585–92. https://doi.org/10.1002/macp.200700514.
[62] Lakovicz JR. Principles of fluorescence spectroscopy. New York, Boston, Dordrecht, Moscow: Kluwer Academic/Plenum; 1996. https://doi.org/10.1007/978-0-387-46312-4.
[63] Currie LA. Detection and quantification limits: origins and historical overview1Adapted from the Proceedings of the 1996 Joint Statistical Meetings (American Statistical Association, 1997). Original title: foundations and future of detection and quantification limits. Contribution of the National Institute of Standards and Technology; not subject to copyright.1. Anal Chim Acta 1999;391:127–34. https://doi.org/10.1016/S0003-2670(99)00105-1.
[64] Analytical Methods. Committee Recommendations for the definition, estimation and use of the detection limit. Analyst 1987;112:199–204. https://doi.org/10.1039/AN9871200199.
[65] Gaussian 09, revision D.01. Wallingford: Gaussian; 2009.

[66] Cramer CJ, Truhlar DG. Density functional theory for transition metals and transition metal chemistry. Phys Chem Chem Phys 2009;11:10757–816. https://doi.org/10.1039/B907148B.
[67] Capobianco A, Borrelli R, Landi A, Velardo A, Peluso A. Absorption band shapes of a Push−Pull dye approaching the cyanine limit: a challenging case for first principle calculations. J Phys Chem A 2016;120:5581–9. https://doi.org/10.1021/acs.jpca.6b05220.
[68] Miertus S, Scrocco E, Tomasi J. Electrostatic interaction of a solute with a continuum. A direct utilizaion of AB initio molecular potentials for the prevision of solvent effects. Chem Phys 1981;55:117–29. https://doi.org/10.1016/0301-0104(81)85090-2.